# Flexural Performance of Reinforced High-Strength Concrete Beams with EAF Oxidizing Slag Aggregates

Sang-Woo Kim[1], Yong-Jun Lee[2], Young-Hyun Lee[3] and Kil-Hee Kim*[4]

[1] Research Assistant Professor, Department of Architectural Engineering, Kongju National University, Cheonan, Republic of Korea
[2] Doctoral Candidate, Department of Architectural Engineering, Kongju National University, Cheonan, Republic of Korea
[3] Assistant, R&D Center, Extpile Co., Ltd., Seoul, Republic of Korea
[4] Professor, Department of Architectural Engineering, Kongju National University, Cheonan, Republic of Korea

**Abstract**

This study evaluates the flexural behavior of reinforced high-strength concrete beams with electric arc furnace (EAF) oxidizing slag aggregates. The main test parameters include the type of aggregates, compressive strength of concrete, and tension reinforcement ratio. A total of eight simply supported beam specimens subjected to four point loads are cast and tested in flexure. Two types of aggregates, natural and EAF oxidizing slag aggregates, are used in this study. The compressive strength of the concrete is designed to have normal- and high-strengths of 24 MPa and 100 MPa, respectively. The tension reinforcement ratios of beam specimens are 0.3 and 0.5 times the balanced reinforcement ratio for flexure. The experimental results indicated that the flexural strength of specimens was not affected by the type of aggregate, whereas the flexural ductility of specimens with EAF oxidizing slag aggregates was superior to that of specimens with natural aggregates, regardless of the compressive strength of concrete and the tension reinforcement ratio.

**Keywords:** electric arc furnace oxidizing slag aggregates; flexural performance; reinforced concrete; high-strength concrete; ductility

## 1. Introduction

In recent years, as environmental pollution and climate change have come to be regarded as important social issues, various efforts have been made to restrict the emission of carbon dioxide, which has been considered to be the main cause of global warming. In the construction industry, the energy consumption for manufacturing cement is considerable; hence, studies on replacing cement have been conducted to reduce the emission of carbon dioxide during its manufacture. Aside from cement, the aggregate that is consumed in huge amounts also causes environmental pollution during the process of collection; therefore, efforts have been continuously made to seek alternatives.

Concrete consists of various materials such as cement, aggregate, water, and admixtures. The recycling of industrial by-product as a material of concrete is an alternative way to reduce energy consumption and the emission of carbon dioxide. The steel industry generates various types of slag as industrial by-product depending on the processes (Manso *et al.* 2004). The use of steel has gradually increased; consequently, industrial by-products have increased every year as well. Fortunately, the recycling of steel slag provides great benefit to the environment because the chemical composition of steel slag is similar to that of construction materials (Rojas and Rojas 2004).

Electric arc furnace (EAF) oxidizing slag, as one of the steel slags, has become highly available for use as an aggregate for concrete owing to its chemical composition consisting of lime (CaO) and silica ($SiO_2$). Hence, it has received attention as a recycling resource for the prevention of environmental pollution and solving the problem of aggregate depletion. The specific gravity of EAF oxidizing slag aggregate is approximately 3.8, which is approximately 1.5 times higher than that of normal natural aggregate (Kim *et al.* 2013). When it is used where high density concrete is required, such as retaining walls, dams, and underground structures, its use value will be high. In addition, it is also applicable where radiation and x-ray shielding are required (Architectural Institute of Japan 2005).

The existing studies on EAF slag have focused on its material properties to obtain the volume stability of slag. Rojas and Rojas (2004) conducted studies on the chemical characteristics of EAF slag; Manso *et*

*Contact Author: Kil-Hee Kim, Professor
Kongju National University
275 Budae-daong, Cheonan, 330-717, Republic of Korea
Tel: +82-41-521-9335 Fax: +82-41-562-0310
E-mail: kimkh@kongju.ac.kr
*( Received October 6, 2015 ; accepted July 13, 2016 )*
DOI http://doi.org/10.3130/jaabe.15.589

*al.* (2004) on its volume stability; and Marroccoli *et al.* (2007) on the raw material of cement and mineral admixture using EAF slag. However, studies focusing on the evaluation of the application to structural members are rare.

Recently, studies on the applicability of EAF oxidizing slag aggregates to structural members have been carried out. Kim *et al.* (2012a, 2012b; 2013; 2014) evaluated the flexural and bond performance of reinforced normal-strength concrete beams and columns with EAF oxidizing slag aggregates. In this study, a flexural test with test variables of the type of aggregate, compressive strength of concrete and tension reinforcement ratio was conducted to evaluate the applicability of EAF oxidizing slag aggregate, one of the by-products of steel slag, to reinforced high-strength concrete members.

## 2. Experimental Program

### 2.1 Materials

The natural and EAF oxidizing slag aggregates were used in this study. The natural coarse and fine aggregates were broken stone and wash aggregate, respectively. The EAF oxidizing slag coarse and fine aggregates were manufactured by crushing. The free CaO content of the slag aggregate was 0.15% with a $CaO/SiO_2$ ratio of 1.51, indicating that it did not run the risk of expansion collapse and satisfied the standards for quality (Architectural Institute of Japan 2005; Korea Standards Association 2011). The specific gravities of the natural coarse and fine aggregates were 2.62 and 2.60, respectively, and the specific gravities of the EAF oxidizing slag coarse and fine aggregates were 3.78 and 3.77, respectively. This indicated that the specific gravity of the EAF oxidizing slag aggregates was approximately 45% higher than that of the natural aggregates.

The mix design of the concrete used in this test is presented in Table 1. The specified concrete strength was designed to 24 and 100 MPa in normal- and high-strength concretes, respectively. To estimate the physical properties of the concrete, concrete cylinders with a diameter of 100 mm and a height of 200 mm were cast while placing the concrete of beam specimens. The typical results of the compressive strength test are shown in Fig.1.(a) and the mean strengths of the concrete cylinders are given in Table 2. In addition, the tests for the modulus of rupture of the concrete with natural and EAF oxidizing slag aggregates were performed to estimate the flexural property of the concrete. The mean modulus of rupture of the concrete used in this study is indicated in Table 2.

In this test, D10 (As = 71.3 $mm^2$) deformed bars with yield strength of 481.5 MPa, elastic modulus of 170.1 GPa, and yield strain of 0.00283 were used for the shear and compressive reinforcement of specimens. For tension reinforcement, D13 (As = 126.7 $mm^2$), D22 (As = 387.1 $mm^2$), and D29 (As = 642.4 $mm^2$) deformed bars with yield strengths of 455.4 ~ 482.8 MPa, elastic modulus of 174.3 ~ 182.0 GPa, and yield strains of 0.00261 ~ 0.00277 were used, as seen in Table 2. The stress versus strain curves of the steel bars used are presented in Fig.1.(b).

### 2.2 Specimen Details and Test Setup

In this study, to compare the flexural behavior of RC beams with different aggregate types, a total of eight specimens with test variables of aggregate types, tension reinforcement ratios, and the compressive strength of concrete were manufactured, as listed in Table 2. The strength of the concrete was designed

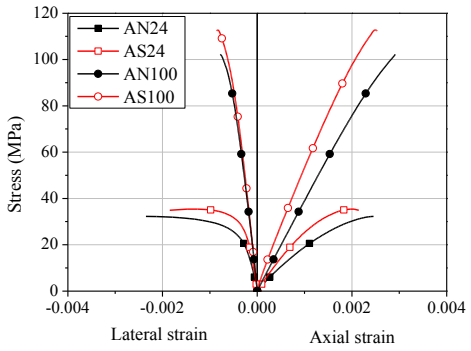


(a) Concrete

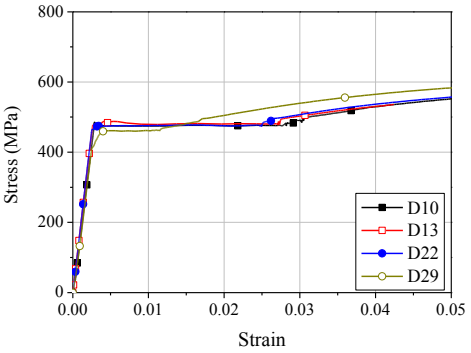


(b) Reinforcement

Fig.1. Stress Versus Strain Relationships of Used Materials

Table 1. Mix Design of Concrete

| Specimens | Design strength (MPa) | W/C (%) | S/a (%) | Unit weight ($kg/m^3$) | | | | | | | |
|---|---|---|---|---|---|---|---|---|---|---|---|
| | | | | W | C | S | G | SF | FA | BFS | AE |
| AN24 | 24 | 57.0 | 49.5 | 175 | 307 | 885 | 853 | - | - | - | 2.15 |
| AS24 | 24 | 55.0 | 48.0 | 177 | 281 | 1240 | 1347 | - | 41 | - | 2.25 |
| AN100 | 100 | 19.2 | 44.5 | 160 | 375 | 596 | 750 | 42 | 84 | 334 | 7.93 |
| AS100 | 100 | 23.4 | 45.0 | 160 | 324 | 944 | 1156 | 36 | 72 | 288 | 5.40 |

Note: SF = Silica fume; FA = Fly-ash; BFS = Blast furnace slag; and AE = Air-entraining agent

Table 2. Properties of Specimens

| Specimens | Aggregates | | $f_c'$ (MPa) | $f_r$ (MPa) | Reinforcement | | |
|---|---|---|---|---|---|---|---|
| | Coarse | Fine | | | Tension | Compression | Shear |
| AN24-0.3 | Natural | Natural | 32.4 | 3.93 | 4-D13 (=0.3$\rho_b$) $f_y$ =482.8 MPa | 2-D10 $f_y$ = 481.5 MPa | D10@70mm $f_y$ = 481.5 MPa |
| AS24-0.3 | Slag | Slag | 34.3 | 4.85 | | | |
| AN24-0.5 | Natural | Natural | 32.4 | 3.93 | 2-D22 (=0.5$\rho_b$) $f_y$ = 476.9 MPa | | |
| AS24-0.5 | Slag | Slag | 34.3 | 4.85 | | | |
| AN100-0.3 | Natural | Natural | 101.7 | 7.49 | 3-D22 (=0.3$\rho_b$) $f_y$ = 476.9 MPa | | |
| AS100-0.3 | Slag | Slag | 107.5 | 8.84 | | | |
| AN100-0.5 | Natural | Natural | 101.7 | 7.49 | 3-D29 (=0.5$\rho_b$) $f_y$ = 455.4 MPa | | |
| AS100-0.5 | Slag | Slag | 107.5 | 8.84 | | | |

Note: $f_c'$ = compressive strength of concrete; $f_r$ = modulus of rupture of concrete; and $\rho_b$ = reinforcement ratio corresponding to balanced strain conditions

to 24 MPa and 100 MPa. The tension reinforcement ratio was determined as 0.3 and 0.5 times that of the balance reinforcement ratio for flexure. In the name of specimens, AN denotes a specimen that only used natural aggregates; AS denotes a specimen that only used EAF oxidizing slag aggregates; 24 and 100 denote the design strengths of used concrete; and 0.3 and 0.5 denote the ratios of the tension reinforcement ratio to the balance reinforcement ratio.

The details of the specimen are shown in Fig.2. The specimens were designed to have a length of 3,080 mm and a cross-section of 200 mm x 300 mm. To prevent shear failure and induce flexural failure, the shear span-to-depth ratio of 4.0 was adjusted to the specimens. Shear reinforcement was provided by a 70 mm space in the flexural test region. To measure the stress and strain states of the reinforcement, strain gauges were attached to the tension, compression, and shear reinforcement, as shown in Fig.2.

To induce a pure flexural region, this study designed the simply supported beam specimens subjected to 4-point loads using a universal testing machine with a 1,000 kN capacity, as shown in Fig.3. The deflection was measured by installing two linear variable differential transformers (LVDTs) at the bottom of the mid-span of the specimen. In addition, to examine the depth of neutral axis and the curvature of specimens, strain gauges for concrete were attached at distances of 0, 10, and 25 mm from the compression fiber at the mid-span of the specimen.

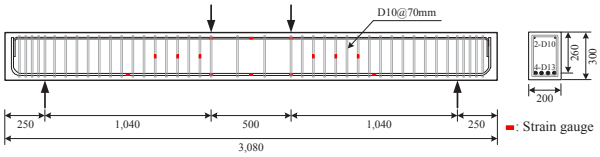


Fig.2. Details of a Typical Specimen

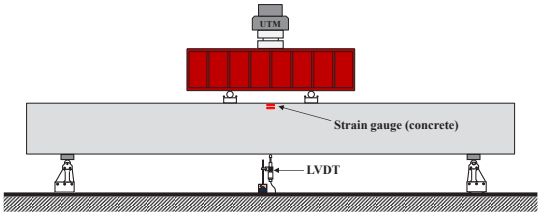


Fig.3. Test Setup of Specimen

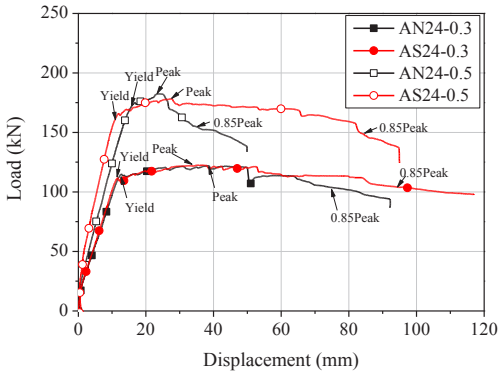


(a) 24-series specimens

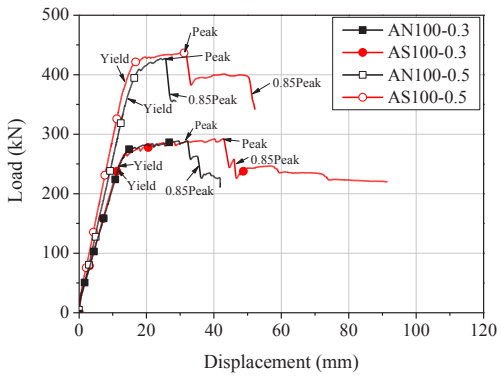


(b) 100-series specimens

Fig.4. Load Versus Displacement Relationships of Specimens

## 3. Experimental Results

### 3.1 General Behavior

Fig.4. shows the load versus displacement relationships of specimens obtained from LVDTs installed at the mid-span of the specimens. As shown in Fig.4., ductile behavior was observed in all specimens after yielding of tension reinforcement. The flexural strength of specimens increased as the concrete compressive strength and the tension reinforcement ratio increased. After peak-load, the flexural capacity reduced owing to the crushing of the extreme compression fiber of concrete, while the flexural cracks at mid-span largely grew. Furthermore, as the concrete

compressive strength increased, the ductile behavior of specimens diminished.

When the tension reinforcement ratio and the grade of concrete compressive strength were the same, the flexural strength of specimens with natural and slag aggregates were similar to each other, as shown in Fig.4. In addition, similar to AN-series specimens with natural aggregates, AS-series specimens with EAF oxidizing slag aggregates exhibited more ductile behavior as the tension reinforcement ratio and the compressive strength of concrete decreased. The strength deterioration of AS24-series specimens after peak-load was relatively slower than that of AN24 specimens. Whereas the strength deteriorations after peak-load for high-strength concrete specimens with natural and slag aggregates were similar to each other.

### 3.2 Crack Patterns

Fig.5. shows the crack patterns of tested specimens when the strain of the extreme compression fiber of the concrete reached 0.003. The crack history of the specimens with EAF oxidizing slag aggregates was similar to that of the specimens with natural aggregates. In the initial loading stage, the first flexural crack occurred at the bottom of the mid-span of each specimen as the load increased. After that, new flexural cracks developed in the pure moment region and spread to both shear spans of all specimens until the tension reinforcement yielded. After the yielding of tension steel bars, cracks in the pure moment region developed upward toward the compression zone of the specimens, whereas those in the shear span grew toward the loading points. After peak-load, the specimens failed in flexure resulting in the crushing of the compression concrete in the pure moment region. The cracks occurring in the specimens developed highly toward the compression zone of the specimens as the tension reinforcement ratio reduced, regardless of the type of aggregate and the compressive strength of concrete.

As shown in Fig.5., the cracks of the specimens with natural aggregates developed more closely to both supports than those of the specimens with EAF oxidizing slag aggregates, regardless of the compressive strength of concrete and the tension reinforcement ratio. This tendency was due to the fact that the modulus of rupture of the concrete with EAF oxidizing slag aggregates was higher than that of the natural aggregate concrete, as described in Table 2. Furthermore, it is noted that the specimens with EAF oxidizing slag aggregates had higher crack control capacity than the specimens with natural aggregates. The crack control capacity of the tested specimens is discussed in more detail in Section 4.4.

## 4. Discussion of Test Results

### 4.1 Flexural Strength

The comparisons of the experimental and analytical results for flexural moments at first yield of tension rebar and ultimate state ($\varepsilon_{cu}$ = 0.003) are presented in Table 3., where $\varepsilon_{cu}$ is the concrete strain of extreme compression fiber at ultimate load. ACI 318-14 (2014) was used for calculating yield moment $M_y$. The ultimate moment $M_u$ was calculated using the equivalent rectangular stress block parameters proposed by ACI 318-14 (2014), CEB-FIP MC90 (1991), CSA A23.3-04 (2004), and NZS 3101-95 (1995), as shown in Table 4.

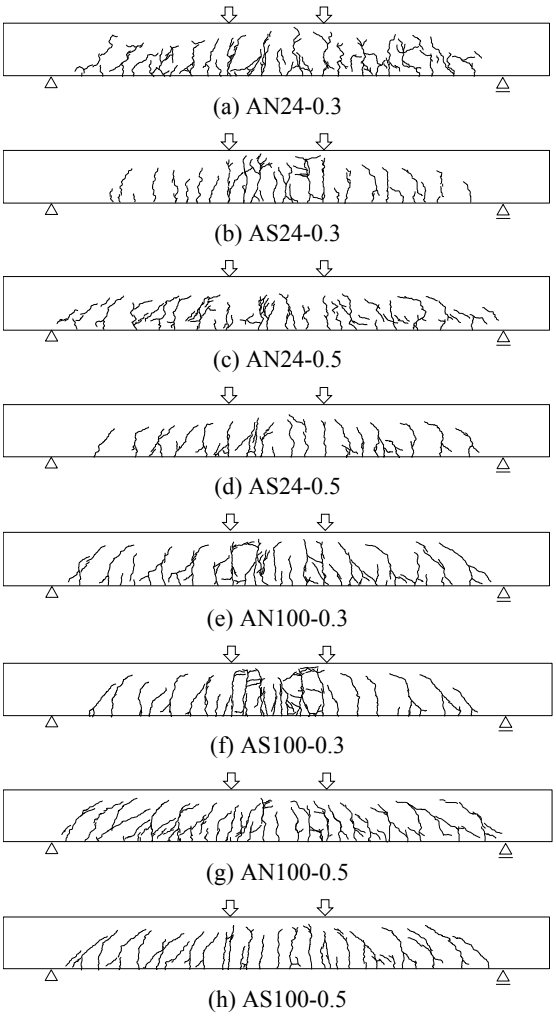


Fig.5. Crack Patterns of Specimens at $\varepsilon_{cu}$ = 0.003

The used equations for calculating moments are as follows:

$$M_y = T\left(d - \frac{kd}{3}\right) \quad (1)$$

$$M_u = \alpha f_c' \beta_1 cb\left(d - 0.5\beta_1 c\right) + A_s' f_s'\left(d - d'\right) \quad (2)$$

where $T$ is the force of tension reinforcement, $d$ is the effective depth of a beam, $kd$ and $c$ are the depth of neutral axis in compression at yield and ultimate states, respectively, $\alpha$ and $\beta_1$ are the coefficient of rectangular stress block, $f_c'$ is the compressive strength of concrete, $b$ is the beam width, $A_s'$ and $f_s'$ are the area and stress of compression reinforcement, respectively, and $d'$ is the distance from the centroid of compression reinforcement to the extreme compression fiber.

Table 3. Comparison between Analytical and Experimental Results for Yield and Ultimate Moments

| Specimens | $f_c'$ (MPa) | Experimental results | | Experimental / Analytical | | | | |
|---|---|---|---|---|---|---|---|---|
| | | | | Yield moment | Ultimate moments | | | |
| | | | | | ACI 318-14 | CEB-FIP MC90 | CSA A23.3-04 | NZS 3101-95 |
| | | $M_{y,\exp}$ $(kN\cdot m)$ | $M_{u,\exp}$ $(kN\cdot m)$ | $\frac{M_{y,\exp}}{M_{y,ana}}$ | $\frac{M_{u,\exp}}{M_{u,ana}}$ | $\frac{M_{u,\exp}}{M_{u,ana}}$ | $\frac{M_{u,\exp}}{M_{u,ana}}$ | $\frac{M_{u,\exp}}{M_{u,ana}}$ |
| AN24-0.3 | 32.4 | 58.4 | 62.5 | 1.04 | 1.03 | 1.04 | 1.03 | 1.03 |
| AS24-0.3 | 34.3 | 57.8 | 61.5 | 1.00 | 1.01 | 1.02 | 1.01 | 1.01 |
| AN24-0.5 | 32.4 | 87.8 | 90.6 | 1.08 | 1.07 | 1.09 | 1.08 | 1.07 |
| AS24-0.5 | 34.3 | 78.1 | 86.3 | 0.94 | 1.02 | 1.03 | 1.02 | 1.02 |
| AN100-0.3 | 101.7 | 129.8 | 148.4 | 1.02 | 1.06 | 1.10 | 1.07 | 1.06 |
| AS100-0.3 | 107.5 | 127.7 | 149.2 | 0.99 | 1.06 | 1.10 | 1.07 | 1.07 |
| AN100-0.5 | 101.7 | 186.2 | 214.0 | 0.97 | 1.04 | 1.11 | 1.06 | 1.05 |
| AS100-0.5 | 107.5 | 196.8 | 220.7 | 1.01 | 1.06 | 1.14 | 1.09 | 1.08 |
| | | | Mean | 1.01 | 1.04 | 1.08 | 1.05 | 1.05 |
| | | | COV | 4.2 % | 2.1 % | 4.0 % | 2.8 % | 2.5 % |

Table 4. Rectangular Stress Block Parameters at Ultimate Strength for Flexure

| Codes | $\alpha$ | $\beta_1$ |
|---|---|---|
| ACI 318-14 | 0.85 | 0.85 (for $f_c' \le 28$ MPa)<br>0.85 - 0.007($f_c'$ - 28) ≥ 0.65 (for $f_c' > 28$ MPa) |
| CEB-FIP MC90 | 0.85 - $f_c'$ / 250 | 1.0 |
| CSA A23.3-04 | 0.85 - 0.0015 $f_c' \ge 0.67$ | 0.977 - 0.0025 $f_c' \ge 0.67$ |
| NZS 3101-95 | 0.85 (for $f_c' \le 55$ MPa)<br>0.85 - 0.004($f_c'$ - 55)≥ 0.75 (for $f_c' > 55$ MPa) | 0.85 (for $f_c' \le 30$ MPa)<br>0.85 - 0.008($f_c'$ - 30) ≥ 0.65 (for $f_c' > 30$ MPa) |

Note: $\alpha$ = width of stress block and $\beta_1$ = ratio of depth of stress block to the distance between neutral axis and extreme compression fiber.

Table 3. indicates the analytical and experimental results for yield and ultimate moments of specimens. The experimental results for yield moment were obtained at the first yield of tension reinforcement. The analytical results for yield moment were calculated using existing sectional analysis for flexure in ACI 318-14 (2014). As seen in Table 3., the analytical result for the yield moment was in good agreement with the test result, with 1.01 on average and 4.2% in coefficient of variation (COV).

The analytical results using stress block parameters for ultimate moment predicted the experimental results with a mean of 1.04 ~ 1.08 and a COV of 2.1% ~ 4.0%. The ACI 318-14 predicted the real ultimate moment most accurately, showing an average ratio of 1.04 and a COV of 2.1%. However, the CEB-FIP MC90 somewhat underestimated test results, as compared to the other equations, showing an average ratio of 1.08 and a COV of 4%. The CSA A23.3-04 and NZS 3101-95 showed approximately the same average ratio of 1.05, and COVs of 2.8% and 2.5%, respectively.

As shown in Table 3., the flexural strength of specimens with EAF oxidizing slag aggregates satisfied the strength required by code equations, regardless of the compressive strength of concrete. In addition, the analytical results calculated by code equations predicted the test results accurately, thereby indicating that the equivalent stress block parameter used for the beams with natural aggregates can be applied to the beams with EAF oxidizing slag aggregates. However, further research for various test variables are needed in order to apply the EAF slag aggregates to structural concrete.

### 4.2 Moment Versus Curvature Relationships

Fig.6. shows the moment-curvature relationship of tested specimens. The theoretical results at first yield and ultimate moment were calculated based on ACI 318-14 (2014) and existing sectional analysis for flexure (Park and Paulay 1975).

The yield and ultimate curvatures can be calculated as follows:

$$\varphi_y = \frac{\varepsilon_y}{d - kd} \tag{3}$$

$$\varphi_u = \frac{\varepsilon_{cu}}{c} = \frac{\varepsilon_{cu}\beta_1}{a} \tag{4}$$

where $\varphi_y$ and $\varphi_u$ are the yield and ultimate curvatures, respectively, and $\varepsilon_y$ is the yield strain of tension steel bars.

Based on Bernoulli's principle, the experimental result for the curvature of specimens was obtained from the strain gauges attached on both the extreme

compression fiber of concrete and the tension reinforcement at mid-span. The analytical ultimate moment and curvature were assumed to be reached when the concrete strain of extreme compression fiber was 0.003.

As shown in Fig.6., the general behavior of the moment versus curvature relationships of tested specimens was similar to that of the load versus deflection ones. The ratios of experimental to analytical results for yield curvature of the specimens with compressive strength of 24 MPa and 100 MPa were 1.08 and 0.98, respectively. This prediction result implies that the analytical results using existing sectional analysis can predict the experimental results accurately. The experimental curvature after yielding of tension reinforcement for several specimens could not be obtained until failure of the specimens owing to the error of strain gauges. The ductility of tested specimens is discussed in detail in Section 4.5 using the displacement ductility factor.

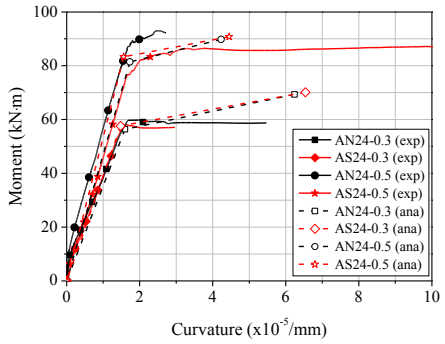


(a) 24-series specimens

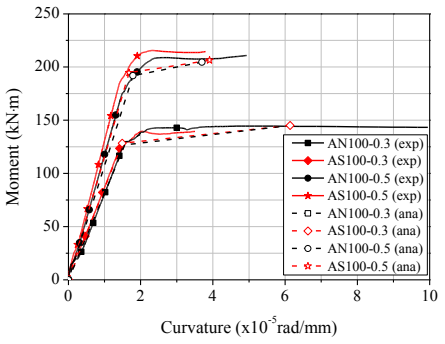


(b) 100-series specimens

Fig.6. Moment Versus Curvature Relationships of Specimens

### 4.3 Variation of Neutral Axis Depth

Fig.7. shows the neutral axis depth ratio versus moment relationships of tested specimens. The neutral axis depth ratio denotes the ratio of the neutral axis depth to effective depth of the specimen. The neutral axis depth was obtained by using the strains measured on the tension and compression reinforcement and the concrete in the compression zone.

As shown in Fig.7., the neutral axis depth ratio tended to decrease after flexural crack occurred. Subsequently, the neutral axis depth was maintained

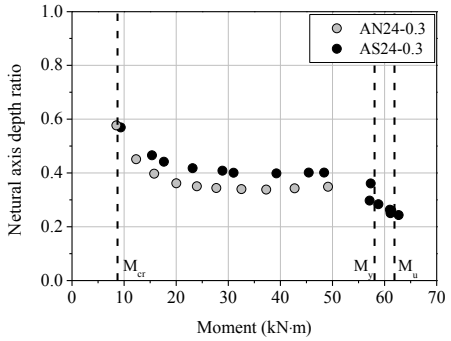


(a) 24-0.3 specimens

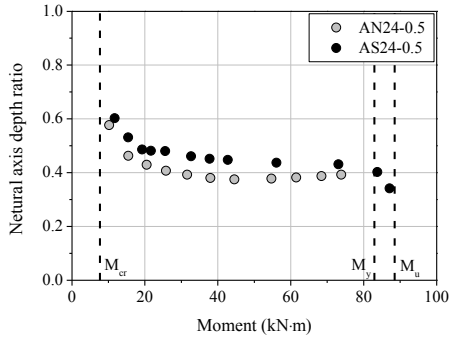


(b) 24-0.5 specimens

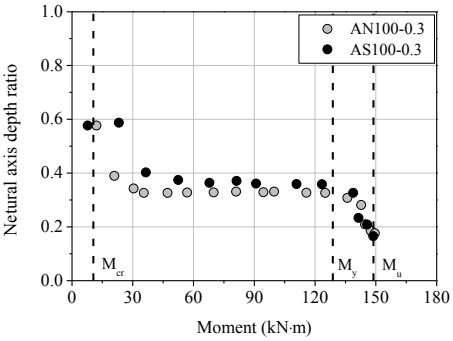


(c) 100-0.3 specimens

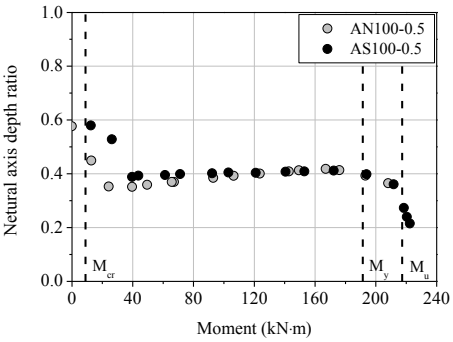


(d) 100-0.5 specimens

Fig.7. Neutral Axis Depth Ratio Versus Moment Relationships

until tension reinforcement yield. After yielding of tension steel bars, the ratio greatly decreased. Furthermore, the neutral axis depth ratio of the specimens with EAF oxidizing slag aggregates increased as tension reinforcement ratio and concrete compressive strength enhanced, similar to natural aggregate specimens. This mechanism represents that the equilibrium condition is successfully established in the specimens with EAF oxidizing slag aggregates.

In the case of 24-series specimens with normal-strength concrete, the specimens with EAF oxidizing slag aggregates had a relatively higher neutral axis depth ratio compared to natural aggregate specimens. This tendency indicates that the crack control capacity of the specimens with EAF oxidizing slag aggregates is superior to the specimens with natural aggregates. In the case of 100-series specimens with high-strength concrete, in contrast, the difference of neutral axis depth ratio on aggregate types decreased compared to 24-series specimens with normal-strength concrete.

### 4.4 Crack Control Capacity

The crack width versus load relationship of specimens is shown in Fig.8. The crack width in Fig.8. denotes the maximum flexural crack width occurring in the pure bending moment region of the specimens. The crack width of AN24-0.5 is not presented in Fig.8. due to errors arising from the measuring instruments. The crack width of tested specimens grew gradually as the load increased, and increased considerably after the tension reinforcement yield. The crack width of AN100-0.5 at peak-load could not be measured during the test because of the brittle failure of the specimen.

24-series specimens with normal-strength concrete satisfied the allowable crack width proposed by KCI 2012 (Korea Concrete Institute 2012), regardless of the type of aggregates. As shown in Fig.8.(a), the difference of crack width at service loads did not appear significant between EAF oxidizing slag aggregates and natural aggregates specimens. AS24-0.3 and AS24-0.5 with EAF oxidizing slag aggregates effectively controlled the cracks until tension reinforcement yielded compared to AN24-0.3 with natural aggregates. In addition, the crack width of AN24-0.3 at peak-load was approximately 2.2 times higher than that of AS24-0.3.

In the case of 100-series specimens with high-strength concrete, the crack widths of all specimens at service loads were less than the maximum crack width required by KCI 2012, such as 24-series specimens. Fig.8.(b) shows that the crack width histories of the specimens are similar to each other, regardless of the type of aggregates.

### 4.5 Ductility Capacity

The comparison results of the ductility capacity of each specimen are shown in Fig.9. The displacement measured from LVDTs installed at the mid-span of each specimen was used for evaluating the ductility capacity of specimens. The definition of the displacement ductility factor used in this study is as follows:

$$\mu_{\Delta,peak} = \frac{\Delta_{peak}}{\Delta_y} \tag{5}$$

$$\mu_{\Delta,85} = \frac{\Delta_{85}}{\Delta_y} \tag{6}$$

where $\Delta_y$ is the displacement at yielding of tension

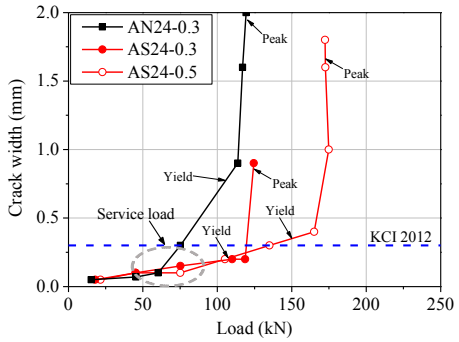


(a) 24-series specimens

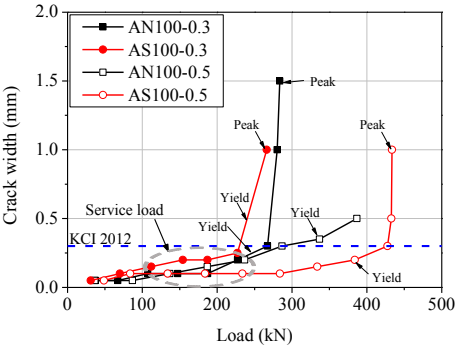


(b) 100-series specimens

Fig.8. Crack Width Versus Load Relationships

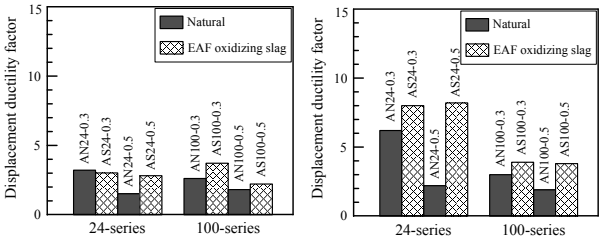


(a) At peak load (b) At ultimate load

Fig.9. Displacement Ductility Factor of Tested Specimens

reinforcement, $\Delta_{peak}$ is the displacement at peak-load, and $\Delta_{85}$ is the displacement corresponding to ultimate load (=0.85$P_{max}$).

As shown in Fig.9., the ductility capacity of the specimens with EAF oxidizing slag aggregates was higher than that of the specimens with natural aggregates for normal- and high-strength concrete. This tendency was significant as the tension reinforcement ratio increased. In the case of specimens with a tension reinforcement ratio of 0.3$\rho_b$, for example, the ultimate ductility factors of the 24- and 100-series specimens with EAF oxidizing slag aggregates was approximately 1.3 times greater than that of the natural aggregate specimens. Whereas, in the case of 0.5$\rho_b$, the ultimate ductility capacity of the slag specimens was superior to the specimens with natural aggregates by approximately 3.9 times for normal-strength concrete and approximately 2.0 times for high-strength concrete. This is because the compression zone in a beam section increases as the tension reinforcement ratio rises. In

other words, the characteristic of compressed concrete is significant as the compression zone increases.

As the tension reinforcement ratio increased, the displacement ductility factor of the AN-series specimens at peak and ultimate loads decreased by up to 64%, whereas AS-series specimens showed little deterioration in ductility capacity. The reason for the high ductility capacity of specimens with EAF oxidizing slag aggregates is due to the fact that the useful limit of the compressive strain for concrete with EAF oxidizing slag aggregates is higher than that of the concrete with natural aggregates.

## 5. Conclusions

From the experimental and analytical investigations carried out on the beams with test variables of the type of aggregates, the compressive strength of concrete, and the tension reinforcement ratio, the following conclusions can be drawn:

(1) The ductile behavior of the slag aggregate specimens was significant as the concrete compressive strength and tension reinforcement ratio decreased, such as the natural aggregate specimens.

(2) The modulus of rupture of the concrete with EAF oxidizing slag aggregate was higher than that of the natural aggregate concrete. This characteristic led the cracks developed in the specimens with EAF oxidizing slag aggregates to not spread and extend more than those of the natural aggregate specimens.

(3) The yield and ultimate moments of the specimens with EAF oxidizing slag aggregates were similar to those of the specimens with natural aggregates, regardless of the compressive strength of concrete and tension reinforcement ratio. The comparison between experimental and analytical results showed that the flexural strength of the specimens with EAF oxidizing slag aggregates could be predicted by using current code equations.

(4) Investigation on the variation of neutral axis depth shows that the equilibrium condition is successfully established in the specimens with EAF oxidizing slag aggregates.

(5) The displacement ductility factor of the specimens with EAF oxidizing slag aggregates was greater than that of the natural aggregate specimens for normal- and high-strength concrete. This tendency was significant as the tension reinforcement ratio of specimens grew.

**Acknowledgments**

This research was supported by the Functional Districts of the Science Belt support program, Ministry of Science, ICT and Future Planning (2015 K000281) and by the National Research Foundation of Korea (NRF) grant funded by the Korea Government (MSIP) (No. NRF-2015R1A2A2A01003 397). This research was also financially supported by the Human Resources Development program (No. 20134010200540) of the Korea Institute of Energy Technology Evaluation and Planning (KETEP) grant funded by the Korea Government Ministry of Trade, Industry and Energy.

## References

1) ACI Committee 318. (2014) Building code requirements for structural concrete (ACI 318-14) and commentary. American Concrete Institute, Farmington Hills, MI.
2) Architectural Institute of Japan. (2005) Recommendation for practice of concrete with electric arc furnace oxidizing slag aggregate. Architectural Institute of Japan, Tokyo, pp.122. (in Japanese)
3) CEB-FIP. (1991) CEB-FIP model code for concrete structures. Comite EURO-International Du Beton.
4) CSA Committee A23.3-04. (2004) Design of concrete structures for buildings CAV3-A23.3-04. Canadian Standards Association, Canada.
5) Kim, S.-W., Kim, Y.-S., Lee, J.-M., and Kim, K.-H. (2013) Structural performance of spirally confined concrete with EAF oxidizing slag aggregate. European Journal of Environmental and Civil Engineering, 17(8), pp.654-674.
6) Kim, S.-W., Lee, Y.-J., and Kim, K.-H. (2012a) Flexural behavior of reinforced concrete beams with electric arc furnace slag aggregates. Journal of Asian Architecture and Building Engineering, 11(1), pp.133-138.
7) Kim, S.-W., Lee, Y.-J., and Kim, K.-H. (2012b) Bond behavior of RC beams with electric arc furnace oxidizing slag aggregates. Journal of Asian Architecture and Building Engineering, 11(2), pp.359-366.
8) Kim, S.-W., Lee, Y.-J., Jung, Y.-J., Lee, J.-Y., and Kim, K.-H. (2014) Applicability of electric arc furnace oxidizing slag aggregates for RC columns subjected to combined bending and axial loads. Materials Research Innovations, 18(S2), pp.793-798.
9) Korea Concrete Institute. (2012) Concrete design code. Korea Concrete Institute, p.342. (in Korean)
10) Korean Standards Association. (2011) Electric arc furnace oxidizing slag aggregate for concrete. Korean Standards Association, Seoul, p.25. (in Korean)
11) Manso, J. M., Gonzalez, J. J., and Polanco, J. A. (2004) Electric arc furnace slag in concrete. ASCE Journal of Materials in Civil Engineering, 16(6), pp.639-645.
12) Marroccoli, M., Nobili, M., Telesca, A., and Valenti, G. L. (2007) Use of electric arc furnace slag as a raw feed component for Portland clinker manufacture. SP242-08, Farmington Hills, MI, American Concrete Institute, pp.91-98.
13) New Zealand Standard. (1995) The design of concrete structures. New Zealand Standard.
14) Park, R. and Paualy, T. (1975) Reinforced concrete structures. John Wiley & Sons Inc., p.769.
15) Rojas, M. F. and Rojas, M. I. S. (2004) Chemical assessment of the electric arc furnace slag as construction material: Expansive compounds. Cement and Concrete Research, 34(10), pp.1881-1888.